AMSR-E/AMSR2 Unified Algorithm – Ocean Suite

Algorithm Theoretical Basis Document

Version 3
November, 2021

Christian Kummerow, David Duncan, David Randel and Paula Brown

TABLE OF CONTENTS

1.0 INTRODUCTION

1.1 Objectives

The AMSR-E and AMSR2 instruments are multichannel passive microwave radiometers flying on the EOS Aqua and GCOM-W1 spacecrafts. As a science mission with integrated applications goals, these sensors will advance understanding of the Earth's water and energy cycle and extend current capabilities in using accurate and timely information of atmospheric moisture to directly benefit the society. The current Algorithm Theoretical Basis Document (ATBD) deals with the ocean product from the AMSR-E and AMSR2 sensors. The passive microwave algorithm uses an optimal estimation approach to derive sea surface Wind Speed (WS), Total precipitable Water (TPW) and Cloud Liquid Water (CLW).

1.2 Purpose

This ATBD describes the AMSR-E/AMSR2 passive microwave ocean algorithm. Output parameters of the algorithm are enumerated in Table 1. This document identifies the physical theory upon which the algorithm is based and the specific sources of input data and output from the retrieval algorithm. The document includes implementation details, as well as the assumptions and limitations of the adopted approach.

Table 1. Key output parameters from the U2 Ocean Product.

Pixel Information		
Parameter	**Units**	**Comments**
Latitude, longitude	Deg.	Pixel earth coordinate position
Quality Flag	None	A measure of the convergence of the OE algorithm
Liquid Water Path	g m^{-2}	Integrated liquid water in the atmospheric column for cloud water only
Total Precipitatable Water	mm	Integrated water vapor
Sun Glint Angle	degrees	Relative angle of reflection between the sun and line of sight of the instrument
Reynolds SST	K	Sea surface temperature from Reynolds OISST
Wind Speed	m s^{-1}	Integrated from retrieved profile

1.3 Scope

This document covers the theoretical basis for the retrieval from the AMSR radiometers. A fully physical, 1D variational inversion algorithm (1DVAR) is used to simultaneously retrieve 'non-raining' parameters such as total precipitable water (TPW), 10m-wind speed, and cloud liquid water path (CLWP) over ocean. Methods were developed for the Global Precipitation Measurement (GPM) Microwave Imager (GMI), but the algorithm is adaptable to any microwave imager due to its fully physical forward model.

Section 1 describes the objectives, purpose and scope of the document. Section 2 provides AMSR-E/AMSR2 satellite instrumentation background. The process concepts and algorithm descriptions for the geophysical parameters of the ocean product are presented in Section 3. Section 4 describes the algorithm infrastructure, while Section 5 summarizes the assumptions and limitations.

2.0 INSTRUMENT CHARACTERISTICS

The AMSR-E instrument is a twelve channel, six frequency total power passive microwave radiometer system. It measures brightness temperatures at 6.925, 10.65, 18.7, 23.8, 36.5, and 89.0 GHz. AMSR2 is very similar instrument, with only one additional channel: 7.3 GHz used for mitigating Radio Frequency interference at 6.9265 GHz. Vertically and horizontally polarized measurements are taken at all channels.

The AMSR-E instrument, modified from the design used for the ADEOS-II AMSR, consists of a 1.6 meter diameter offset parabolic reflector (2.0 meters for AMSR2) fed by an array of six feedhorns. The reflector and feedhorn arrays are mounted on a drum, which contains the radiometers, digital data subsystem, mechanical scanning subsystem, and power subsystem. The reflector/feed/drum assembly is rotated about the axis of the drum by a coaxially mounted bearing and power transfer assembly. All data, commands, timing and telemetry signals, and power pass through the assembly on slip ring connectors to the rotating assembly.

A cold load reflector and a warm load are mounted on the transfer assembly shaft and do not rotate with the drum assembly. They are positioned off axis such that they pass between the feedhorn array and the parabolic reflector, occulting it once each scan. The cold load reflector reflects cold sky radiation into the feedhorn array thus serving, along with the warm load, as calibration references for the AMSR-E/AMSR2. Calibration of the radiometers is essential for collection of useful data. Corrections for spillover and other antenna pattern effects are incorporated in the data processing algorithms.

The AMSR-E rotates continuously about an axis parallel to the local spacecraft vertical at 40 rpm. At an altitude of 705 km (700km for AMSR2), it measures the upwelling scene brightness temperatures over an azimuthal range of +/- 70 degrees about the sub-satellite track, resulting in a swath width of 1500 km (1450km for AMSR2).

During a period of 1.5 seconds the spacecraft sub-satellite point travels 10 km. Even though the instantaneous field-of-view for each channel is different, active scene measurements are recorded at equal intervals of 10 km along the scan. To produce complete images at 89 GHz where the IFOV (5x5km) is smaller than the separation between scan lines, both AMSRs uses an offset 89 GHz channel (89B) that scans

between the all-channel scan lines with an offset of 5 km. The half cone angle at which the reflector is fixed is 46.6 degrees which results in an Earth incidence angle of 53.8 degrees (AMSR2: 47.5 and 55.0 degrees). Table 2 lists the pertinent performance characteristics.

Table 2. AMSR-E and AMSR2 PERFORMANCE CHARACTERISTICS

AMSR-E							
Center Frequency (GHz)	6.925		10.65	18.7	23.8	36.5	89.0
Bandwidth (MHz)	350		100	200	400	1000	3000
Sensitivity (K)	0.34		0.7	0.7	0.6	0.7	1.2
IFOV(km x km)	75 x 43		51 x 29	27 x 16	32 x 18	14 x 8	6 x 4
Sampling rate (km x km)	10 x 9		10 x 9	10 x 9	10 x 9	10 x 10	5 x 5
Integration Time (msec)	2.5		2.5	2.5	2.5	2.5	1.2
Main Beam Efficiency (%)	95.3		95.0	96.3	96.4	95.3	96.0
Beamwidth (degrees)	2.2		1.5	0.8	0.92	0.42	0.19
AMSR2							
Center Frequency (GHz)	6.925	7.3	10.65	18.7	23.8	36.5	89.0
Bandwidth (MHz)	350	350	100	200	400	1000	3000
Sensitivity (K)	0.34	.43	0.7	0.7	0.6	0.7	1.4
IFOV(km x km)	62 x 35	62 x 35	42 x 24	22 x 14	26 x 15	12 x 7	5 x 3
Sampling rate (km x km)	10 x 10	10 x 10	10 x 10	10 x 10	10 x 10	10 x 10	5 x 5
Integration Time (msec)	2.6	2.6	2.6	2.6	2.6	2.6	1.3
Main Beam Efficiency (%)	>90.0	>90.0	>90.0	>90.0	>90.0	>90.0	>90.0
Beamwidth (degrees)	1.8	1.8	1.2	0.65	0.75	0.35	0.15

It should be noted that while AMSR-E and AMSR2 are very similar instruments, and use the same retrieval algorithm, the brightness temperatures provided in the Level 1B product used as input to the retrieval algorithm are not fully consistent. To avoid introducing Inconsistencies in the geophysical parameters, Tb for both AMSR-E and AMSR2 are shifted to be consistent with the GPM GMI radiometer as defined by the GPM Intercalibration Working Group (Berg et al., 2016).

3.0 ALGORITHM DESCRIPTION

3.1 Ocean Algorithm (from Duncan and Kummerow, 2016)

The oceanic parameters of TPW, 10m wind speed, and CLWP are termed 'non-raining' because, historically, microwave radiative transfer models can quickly and fairly accurately model radiances in an absorbing/emitting atmosphere, but the scattering of microwave radiation by precipitation is more difficult and remains an ongoing problem [*Weng*, 2007]. In fact, most satellite observations in areas of precipitation, and indeed cloud, are not assimilated into global weather models and constitute an active area of research [*Bauer et al*., 2006; *Bennartz and Greenwald*, 2011]. The non-raining parameters are thus geophysical variables retrievable from a passive microwave platform in clear-sky or cloudy conditions, but not in precipitating or scattering conditions; to retrieve in raining conditions, assumptions have to be made about partitioning cloud water and rainwater, as in *Hilburn and Wentz* [2008], and the radiative transfer is more complicated.

Ability to retrieve the non-raining parameters from passive microwave radiances derives from the emission/absorption characteristics of water vapor and liquid water at microwave frequencies and the effect of wind speed on the emissivity of the ocean. To first order, the emission of the ocean surface at microwave frequencies is dependent on wind speed and temperature alone; other factors like ocean salinity and wind direction are second-order effects [*Meissner and Wentz*, 2002]. By assuming a vertical profile of water vapor and cloud water, as well as a temperature profile, the atmosphere can be adequately modeled at microwave frequencies, and thus the non-raining parameters can be retrieved. Highly variable atmospheric constituents such as aerosols and ozone are ignored due to their small radiative impacts.

Retrieval algorithms for microwave imagers have historically relied upon statistical methods [*Wilheit and Chang*, 1980; *Alishouse et al*., 1990], and semi-physical methods [*Liu et al*., 1992; *Greenwald et al*., 1993; *Wentz*, 1997] to determine some or all of the non-raining parameters over ocean. Though empirical and semi-physical methods are still widely used, retrieval algorithms have generally moved towards simultaneous retrieval of all non-raining parameters [Boukabara et al., 2011]. In addition to increased

computational power, this is due to the interdependence of microwave frequencies on surface emissivity and emission from both water vapor and cloud water, and is thus the best way to ensure that the resultant output is consistent with the observed radiances. *Elsaesser and Kummerow* [2008], hereinafter *EK08*, utilized the mathematical framework outlined in *Rodgers* [2000] to iteratively solve for all parameters simultaneously, and it is this approach that is built upon here.

In the last decade or more, efforts have moved from sensor-specific approaches to an emphasis on intercalibration and algorithms that can provide consistent time series of geophysical constituents from multiple satellite sensors [*Berg et al*., 2013; *Robertson et al*., 2014; *Hou et al*., 2014]. The approach detailed here follows previous studies that iteratively solve for geophysical parameters by forward modeling the atmosphere and finding a solution that closely matches observed radiances, balancing observations with prior knowledge of the state vector [*Deblonde and English,* 2003; *Bettenhausen et al*., 2006; *EK08*; *Boukabara et al*., 2011; *Munchak and Kummerow*, 2011]. The 1D variational (1DVAR) approach is generalizable to other sensors due to its fully physical forward model. The process of forward modeling and iterating to find a solution that minimizes differences between observed and simulated radiances, while taking prior information into account, adds constraints to the under-constrained problem. The forward model must contain all atmospheric components to which the radiances are significantly sensitive and simulate the atmospheric profile of absorbing/emitting constituents with enough fidelity to satisfy the weighting functions of all channels. Any combination of channels may be used in the iteration, the radiative transfer and emissivity models may be swapped, and prior information can be weighted heavily or not at all, lending the approach great flexibility.

The remainder of this paper is organized as follows. Section two lists the data sources employed for algorithm development and validation; section three gives a brief overview of 1DVAR theory, details the CSU 1DVAR's forward model, and describes calculation of the covariance matrices; section four contains results and validation against independent datasets; section five discusses sensitivities of the algorithm; and section six contains discussion and some conclusions.

3.1.1 1DVAR

At the heart of the retrieval is the mathematical framework known as a one-dimensional variational (1DVAR) technique, also known as optimal estimation. While the mathematics of this technique is described in detail in numerous places [*Rodgers*, 2000; *Bettenhausen et al*., 2006; *EK08*; *Boukabara et al*., 2011], it is critical to the retrieval and thus warrants a quick overview.

1DVAR is a matrix-based inverse method predicated upon Bayes' Theorem. It blends observations, prior environmental knowledge, and knowledge of the errors in both to invert the measurement vector **y** to determine the state vector **x**. In this case, **y** is a vector of brightness temperatures from GMI and **x** is a vector that includes CLWP, wind speed, and atmospheric water vapor. The measurements are related to the geophysical state by a forward model, **f(x,b)**, that is dependent upon elements in the state vector and also assumed geophysical properties, **b**. In this case, the forward model is described in Section 3.2 and **b** constitutes the atmospheric temperature profile, wind direction, surface salinity, and everything else not solved for explicitly.

The covariancess in the measurement vector are described by matrix $\mathbf{S_y}$, and covariances in the a priori vector, $\mathbf{x_a}$, that describe prior knowledge of the state vector is given by matrix $\mathbf{S_a}$. The inversion is solved iteratively via Newton's method by assuming Gaussian-distributed errors and a moderately linear response of the measurements to changes in the state vector [*Rodgers*, 2000]. To solve the inverse problem, we minimize a cost function that weights both measurements and prior knowledge in accordance with their uncertainties:

$$\Phi = (x-x_a)^T S_a^{-1}(x-x_a) + [y-f(x,b)]^T S_y^{-1}[y-f(x,b)].$$

The minimum gradient of Φ with respect to **x** describes the maximum probability solution of **x** given measurement **y**. This formalism produces a posterior probability density function (PDF) of the retrieved state, described by

$$S_x = (K^T S_y^{-1} K + S_a^{-1})^{-1},$$

where **K** is the weighting function matrix or Jacobian that describes the first derivative of each forward modeled element to changes in the state vector. Elements of the $\mathbf{S_x}$ matrix describe the estimated variances and covariances of errors for retrieved parameters.

Convergence is defined by a minimized cost function and simulated Tbs that change very little between iterations (given as equation 5.33 in *Rodgers* [2000]). Convergence is typically reached in two iterations for clear-sky scenes and 3-5 iterations for cloudy scenes. A normalized chi-squared metric is used to examine quality of convergence,

$$\chi^2 = [y\text{-}f(x,b)]^T S_y^{-1} [y\text{-}f(x,b)] / N_{chan},$$

where N_{chan} is the number of satellite channels used. The χ^2 cost function referred to throughout the paper is thus the part of Φ that signals the fit to the observations and is independent of the prior. χ^2 is normalized by N_{chan} to allow greater adaptability to other sensors and channel combinations.

3.1.2 Forward model

The forward model employs the Community Radiative Transfer Model, CRTM [*Liu and Weng*, 2013] to compute simulated radiances at the GMI frequencies. Surface emissivities come from the FASTEM6 ocean surface emissivity model [*Kazumori and English*, 2015]. The CSU 1DVAR version described here uses CRTM Release 2.2.1. The forward model has 16 vertical layers in pressure, from 100hPa to the surface. The lowest layer's depth varies in accordance with sea level pressure from the analysis data, while the other layers are static.

The EOF-based approach of retrieving the water vapor profile is a compromise between allowing the channels' weighting functions to guide the retrieved distribution of water vapor and requiring prior information to make the problem viable. This is a common method to reduce dimensionality in 1DVAR retrievals [*Boukabara et al*., 2011; *Munchak et al*., 2016]. To guide the retrieval, the a priori profiles are subset by SST. The EOFs are defined as variations around a mean profile, calculated offline from ERA-Interim data. The 1DVAR process solves for the coefficient of each EOF, which may be positive or negative, yielding a profile that best matches the Tb vector,

$$WV_{ret} = WV_{SST} + c_1 EOF_{SST,1} + c_2 EOF_{SST,2} + c_3 EOF_{SST,3}.$$

An advantage of EOFs is no covariance between the principal components, by definition, setting off-diagonal elements of the $\mathbf{S_a}$ matrix to zero. According to analysis of ERA-Interim data, the first three EOFs of water vapor mixing ratio account for 90-98% of the

total variability, depending on the SST regime. The number of EOFs employed could be increased or decreased for different channel combinations, but for GMI using three EOFs is optimal.

Both wind direction and the atmospheric temperature profile are taken from ERA-Interim. Wind direction has a small but significant effect on Tbs that increases with wind speed and depends on frequency. Instead of solving for wind direction, which has a weak radiometric signal [*Wentz*, 1992], wind direction is taken from ERA-Interim. Its inclusion removes cross-scan artifacts that are present if a static wind direction is assumed. The channel suite of GMI does not contain any temperature sounding channels, and therefore the temperature profile is also taken from the model. The CSU 1DVAR can be run without this model guidance, but assumed channel errors need to be increased if using a climatological lapse rate. Sea surface salinity is taken from monthly climatologies derived from Aquarius mission data [Le Vine et al., 2015].

Other assumptions in the forward model include a fixed cloud layer, no scattering due to clouds or aerosols, a fixed cloud drop size distribution, and a plane-parallel atmosphere. The significance of the plane-parallel assumption is not assessed here but has been explored elsewhere [*Rapp et al*., 2009; *Bennartz and Greenwald*, 2011]; FOV inhomogeneity is a source of retrieval error for Tbs that have not been convolved to a common resolution. This is potentially a significant source of error for broken cloud fields in particular, given the size differential between 36GHz and 166GHz FOVs, for example. Placement of the cloud layer has little impact on the retrieval due to the increasing emissivity of cloud drops with decreasing temperature [*Mätzler et al*., 2010], causing the effective emission to be somewhat independent of cloud height but tied strongly to the total amount of liquid water in the column. Pixels for which the non-scattering assumption is invalid typically lead to non-convergence and often signal areas of precipitation, explored in Section 4. If the cloud is non-precipitating, due to cloud drops being in the Rayleigh regime for microwave frequencies, emission is proportional to column liquid water mass [*Bennartz*, 2007], and thus the droplet size assumption is not significant.

3.1.3 Determination of S_y and S_a

The matrices $\mathbf{S_a}$ and $\mathbf{S_y}$ especially have a large impact on the 1DVAR retrieval. $\mathbf{S_a}$ represents the best estimate of prior knowledge of the state vector, and can thus come from a variety of sources. For example, *Boukabara et al*. [2011] use output from various global and mesoscale models, whereas *EK08* defines global variances of each retrieved parameter from climatology and assumes zero covariances for all. Determination of $\mathbf{S_y}$ is much more nuanced.

Elements of $\mathbf{S_y}$ essentially inform the algorithm how much weight each channel should be given in the inversion. This includes sensor noise, forward model parameter error, and the error introduced by the forward model, with the latter the dominant term. In *EK08* this was estimated in a piecewise manner, adding sensor noise (noise-equivalent differential temperature, NEDT) to estimates of channel sensitivity taken from perturbations to parts of the forward model. In contrast, *Boukabara et al*. [2011] model radiances through ECMWF model output and then scale the resultant uncertainties by uncertainties in the geophysical input values themselves. This also serves as a method of bias correction, essentially forcing the radiances to match the model, a method common in satellite data assimilation [*Liu and Boukabara*, 2014], though variational methods are now common for bias correction in data assimilation as well [*Auligne et al*., 2007].

In this study, $\mathbf{S_a}$ is largely determined via analysis of 6-hourly ERA-Interim data. For wind speed, climatological maps of standard deviations yield location- and month-dependent values. These values are calculated at the N128 model grid resolution and then interpolated and smoothed to produce a high-resolution global grid. In contrast, the EOFs of water vapor are allowed to move more freely, constrained weakly by the variability observed in the reanalysis data, but subset only by SST so as not to alias any regional biases of the model into the retrieval. Each EOF coefficient has maximum and minimum values of 4 and -4, so as to limit unphysical behavior.

For liquid water there is less constraint, with the prior and variance globally defined in logarithm space; this permits the retrieval to solve for a multitude of clear-sky scenes without biasing against high CLWP regimes, as the global distribution of CLWP is far from Gaussian but is more so in logarithm space. The relatively strong radiometric signal of liquid water thus guides the inversion instead of prior information, with no reliance upon model data. Winds and water vapor, in contrast, have subtler radiometric

signals and therefore benefit from greater constraint. The only off-diagonal elements of $\mathbf{S_a}$ that are significant, and thus taken into account, are covariances between CLWP and the EOFs of water vapor, which come from the reanalysis. The results are fairly insensitive to whether $\mathbf{x_a}$ comes from a model or climatology, but assumed errors need to be increased if using climatology and the results are noisier.

Calculation of $\mathbf{S_y}$ begin with Tbs being forward modeled using ERA-Interim data at their native vertical resolution, 37 pressure levels, including ice and water clouds as well as scattering in the radiative transfer. This is then compared to simulated radiances, again from ERA-Interim, but using the simplified forward model of the retrieval—16 vertical pressure levels, the EOF-based water vapor profile described in Section 3.2, a fixed cloud layer, and no cloud ice. To account for forward model parameter error—the uncertainty of prescribed elements (**b**) in the forward model—noise is added to the parameters of SST, salinity, wind direction, and the temperature profile when running the simplified forward model. Specifically, the uncertainties are taken to be 0.62K for SST, 0.5psu for salinity, 20 degrees for wind direction, and 2K for temperature. Around a hundred millions points are forward modeled using both sets of assumptions to get a large statistical sample.

The difference in Tb, simulated versus simulated, is then a synthetic dataset that speaks to forward model error, including forward model parameter error, in an imperfect but tractable way. This method attempts to account for the largest forward model error sources, however some error sources, such as absorption model or FOV inhomogeneity errors, cannot readily be quantified. After careful screening for bad matchups and contamination from precipitation or sea ice, the covariances of these simulated versus simulated Tb differences yield an estimate of the forward model errors. This approach also yields forward model biases, typically ~0.1K for low frequencies and 1-4K for the 183GHz channels, which are applied to the observed Tbs prior to processing.

In order to account for emissivity model errors, a separate analysis compared the Tb response of FASTEM6 at AMSR frequencies against another state-of-the-art emissivity model, *Meissner and Wentz* [2012]. Covariances of the difference between the two models are taken as a proxy for emissivity model uncertainty. These covariances are added to those from the previous analysis. Lastly, NEDT values are added to the diagonal

elements of $\mathbf{S}_y$ from this analysis to yield the channel error covariance matrix used in the algorithm, shown in Figure 1.

It should be stressed that small differences in $\mathbf{S}_y$ can cause large differences in the performance of the retrieval. Decreasing the diagonal elements by say 20% markedly decreases the number of pixels that reach convergence, whereas overestimating $\mathbf{S}_y$ will cause the retrieval to over-weight the prior. Typically, this sensitivity most affects convergence in cloudy scenes, consistent with *Bormann et al*. [2011], whereas convergence can occur in some clear-sky scenes when assuming that $\mathbf{S}_y$ is simply NEDT. The method described for calculating $\mathbf{S}_y$ yields channel errors and their covariances related to the forward model, but it does not take every possible error source into account and thus may need to be adjusted for different applications and especially for other sensors that may not be as well calibrated as GMI. As seen in Figure 2, histograms of Tb residuals (observed minus simulated Tb) for each channel are largely Gaussian and exhibit maxima near zero.

Figure 1. Channel error covariance matrix, given as the square root of the covariances so as to be in units of Kelvin. Negative covariances are shown as -1 times the square root of the absolute value of the covariance so as to aid interpretation. This represents the calculated forward model error plus the published NEDT values along the diagonal.

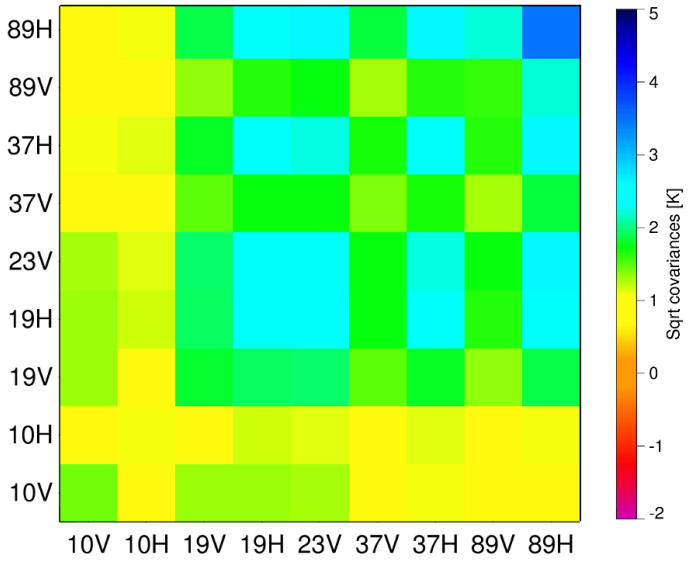

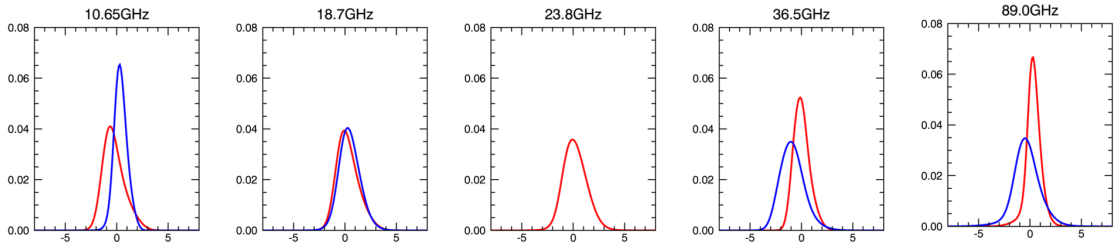

Figure 2. Histograms of Tb residuals (observed minus simulated Tb) for 10 channels of AMSR, comprised of all converged pixels over one month. Red signifies V polarization, blue H polarization.

4.0 Output Variables and Flags

4.1 Orbit Header Record Variable Specifications

Num Scans, Num Pixels
Number of Scans, Pixels in each scan

4.2 Scan Data Record Variable Specifications

Time
year, month, day, hr, min, sec

Latitude, Longitude
Scan latitude and longitude.

4.3 Pixel Data Record Variable Specifications

Latitude, Longitude
Pixel latitude and longitude.

quality Flag
qualityFlag indicates a generalized quality of the retrieved pixel.

Valid values include:
0 : Highest_quality_retrieval
1 : Convergence_reached
2 : No_convergence_precipitation_or_land_contamination_possible
3 : TPW_quality_check_failed_set_to_missing
4 : Sun_glint_angle_less_than_20_degrees_set_to_missing
5 : Not_run_due_to_land_or_sea_ice"

chi Squared
Error diagnostic for Optimal Estimation calculation of TPW and wind speed. Values greater than the number of channels (9 for TMI) should be considered suspect, with values greater than 18 of limited use. Rainfall is possible above these values. Values could range from 0 to 10000, but should be less than 100.

Land Percentage
A surface variable, in percent, defining the fraction of land.

sun Glint Angle
Conceptually, the angle between the sun and the instrument view direction as reflected off the Earth's surface. More specifically, define a Sun Vector from the viewed pixel location on the earth ellipsoid-model surface to the sun. Also define an Inverse Satellite Vector from the pixel to the satellite. Then reflect the Inverse Satellite Vector off the earth's surface at the pixel location to form the Reflected Satellite View Vector. sunGlintAngle is the angular separation between the Reflected Satellite View Vector and the Sun Vector. When sunGlintAngle is zero, the instrument views the center of the specular (mirror-like) sun reflection.

Reynolds Sea Surface Temperature
Reynolds SST for this pixel.

total Precipitable Water
Liquid equivalent of the total water vapor in the atmospheric column.

wind Speed
Wind speed at the 10 meters above sea surface derived from the OE retrieval.

Liquid Water Path
The liquid water path derived from the OE retrieval of non-raining parameters.

Error of Wind speed, LWP and TPW
Posterior error for wind speed, LWP and TPW variables, given as the standard deviation of errors.

5. 0 REFERENCES

Alishouse, J. C., S. A. Snyder, J. Vongsathorn, and R. R. Ferraro (1990), Determination of oceanic total precipitable water from the SSM/I, IEEE Trans. Geosci. Rem. Sens., 28, 811–816.

Auligné, T., McNally, A. P. and Dee, D. P. (2007), Adaptive bias correction for satellite data in a numerical weather prediction system, Q. J. R. Meteorol. Soc., 133, 631–642, doi:10.1002/qj.56

Bauer, P., P. Lopez, A. Benedetti, S. Saarinen, E. Moreau (2006), Implementation of 1D+4D-Var assimilation of precipitation-affected microwave radiances at ECMWF, II: 4D-Var, Q. J. Roy. Meteor. Soc., 132, 2307-2332.

Bennartz, R. and T. Greenwald (2011), Current problems in scattering radiative transfer modeling for data assimilation, Q.J.R. Meteorol. Soc., 137, 1952-1962.

Bennartz, R. (2007), Global assessment of marine boundary layer cloud droplet number concentration from satellite, J. Geophys. Res., 112, D02201, doi:10.1029/2006JD007547.

Berg, W., M. Sapiano, J. Horsman, and C. Kummerow (2013), Improved geolocation and Earth incidence angle information for a fundamental climate data record of the SSM/I sensors, IEEE Trans. Geosci. Rem. Sens., 51, 1504-1513.

Berg, W., S. Bilanow, R. Chen, S. Dattta et al., (2016). Intercalibration of the GPM Microwave Radiometer Constellation. *J. Atmos. And Oceanic Tech.*, **33**, DOI: 10.1175/JTECH-D-16-0100.1

Bettenhausen, M. H., C. K. Smith, R. M. Bevilacqua, N. Wang, P. W. Gaiser, and S. Cox (2006), A nonlinear optimization algorithm for WindSat wind vector retrievals, IEEE Trans. Geosci. Rem. Sens., 44(3), 597-610.

Bormann, N., A. J. Geer, and P. Bauer (2011), Estimates of observation-error characteristics in clear and cloudy regions for microwave imager radiances from numerical weather prediction, Q. J. R. Meteorol. Soc., 137, 2014–2023, doi:10.1002/qj.833.

Boukabara, S.-A., and Coauthors (2011) MiRS: An all-weather 1DVAR satellite data assimilation and retrieval system, IEEE Trans. Geosci. Rem. Sens., 49(9), 3249–3272, doi:10.1109/TGRS.2011.2158438.

Deblonde, G. And S. English (2003), One-Dimensional variation retrievals from SSMIS-simulated observations, J. Appl. Meteor., 42, 1406-1420, doi:10.1175/1520-0450(2003)042<1406:OVRFSO>2.0.CO;2.

Draper, D., D. Newell, F. Wentz, S. Krimchansky, and G. Skofronick-Jackson (2015), The global precipitation measurement (GPM) microwave imager (GMI): Instrument overview and early on-orbit performance, IEEE J. Sel. Top. Appl. Earth Obs. Rem. Sens., 8(7), 3452-3462, doi:10.1109/JSTARS.2015.2403303.

Duncan, D. I., and C. D. Kummerow (2016), A 1DVAR retrieval applied to GMI: Algorithm description, validation, and sensitivities, J. Geophys. Res. Atmos., 121, 7415–7429, doi:10.1002/ 2016JD024808.

Elsaesser, G. S., and C. D. Kummerow (2008) Toward a fully parametric retrieval of the nonraining parameters over the global oceans, J. Appl. Climatol., 47, 1599-1618.

Greenwald, T. J., G. L. Stephens, T. H. Vonder Haar, and D. L. Jackson (1993), A physical retrieval of cloud liquid water over the global oceans using special sensor microwave/imager (SSM/I) observations, J. Geophys. Res., 98, 18471–18488.

Hilburn, K. A., and F. J. Wentz (2008), Intercalibrated passive microwave rain products from the unified microwave ocean retrieval algorithm (UMORA), J. Appl. Meteor. Climatol., 47, 778–794.

Hou, A. Y., and Coauthors (2014), The Global Precipitation Measurement mission, Bull. Amer. Meteor. Soc., 95, 701–722.

Kazumori, M. and S. J. English (2015), Use of the ocean surface wind direction signal in microwave radiance assimilation, Q. J. R. Meteorol. Soc., 141, 1354–1375, doi:10.1002/qj.2445.

Kummerow, C. D., S. Ringerud, J. Crook, D. Randel and W. Berg, 2010. An observationally generated *A-Priori* database for microwave rainfall retrievals, *J. Atmos. and Oceanic Tech.*, **28(2)**, 113-130, doi: 10.1175/2010JTECHA1468.1.

Le Vine, D. M., E. P. Dinnat, T. Meissner, S. H. Yueh, F. J. Wentz, S. E. Torrusio, and G. Lagerloef (2015), Status of Aquarius/SAC-D and Aquarius salinity retrievals, J. Sel. Topics Appl. Earth Obs. Rem. Sens., 8(12), 5401-5415, doi:10.1109/JSTARS.2015.2427159.

Liu, Q. and S. Boukabara (2014), Community radiative transfer model (CRTM) applications in supporting the Suomi National Polar-orbiting Partnership (SNPP) mission validation and verification, Remote Sens. Env., 140, 744-754, doi:10.1016/j.rse.2013.10.011.

Liu, W. T., W. Tang, and F. J. Wentz (1992), Precipitable water and surface humidity over global oceans from special sensor microwave imager and European center for medium range weather forecasts, J. Geophys. Res., 97(C2), 2251-2264.

Mätzler, C., P. W. Rosenkranz, and J. Cermak (2010), Microwave absorption of supercooled clouds and implications for the dielectric properties of water, J. Geophys. Res., 115, D23208, doi:10.1029/2010JD014283.

Meissner, T. and F. J. Wentz (2002), An updated analysis of the ocean surface wind direction signal in passive microwave brightness temperatures, IEEE Trans. Geosci. Remote Sens., 40(6), 1230–1240.

Meissner, T., and F. Wentz (2012), The emissivity of the ocean surface between 6 and 90 GHz over a large range of wind speeds and earth incidence angles, IEEE Trans. Geosci Remote Sens., 50(8), 3004–3026, doi:10.1109/TGRS.2011.2179662.

Munchak, S. J., and C. D. Kummerow (2011), A modular optimal estimation method for combined radar-radiometer precipitation profiling, J. Appl. Meteor. Climatol., 50, 433–448.

Munchak, S. J., R. Meneghini, M. Grecu, and W. Olson (2016), A consistent treatment of microwave emissivity and radar backscatter for retrieval of precipitation over water surfaces, J. Atmos. Ocean. Tech., 33, 215-229, doi:10.1175/JTECH-D-15-0069.1.

Rapp, A. D., M. Lebsock, and C. Kummerow (2009), On the consequences of resampling microwave radiometer observations for use in retrieval algorithms, J. Appl. Meteor. Climatol., 48, 1981-1993, doi:10.1175/2009JAMC2155.1.

Robertson, F.R., M.G. Bosilovich, J.B. Roberts, R.H. Reichle, R. Adler, L. Ricciardulli, W. Berg, and G.J. Huffman (2014), Consistency of estimated global water cycle variations over the satellite era, J. Climate, 27, 6135–6154, doi:10.1175/JCLI-D-13-00384.1.

Rodgers, C. D. (2000), Inverse Methods for Atmospheric Sounding: Theory and Practice,

World Scientific Publishing Co., Singapore.
Weng, F. (2007), Advances in radiative transfer modeling in support of satellite data assimilation, J. Atmos. Sci., 64, 3799-3807, doi:10.1175/2007JAS2112.1.
Wentz, F. J. (1992), Measurement of oceanic wind vector using satellite microwave radiometers, IEEE Trans. Geosci. Rem. Sens., 30(5), 960–972, doi:10.1109/36.175331.
Wentz, F. J., L. Ricciardulli, K. Hilburn, and C. Mears (2007), How much more rain will global warming bring?, Science, 317, 233-235.
Wilheit, T. T., and A. T. C. Chang (1980), An algorithm for retrieval of ocean surface and atmospheric parameters from the observations of the scanning multichannel microwave radiometer, Radio Science, 15(3), 525–544, doi:10.1029/RS015i003p00525.